



This is a repository copy of *Performance evaluation of spatial scattering modulation in the indoor environment*.

White Rose Research Online URL for this paper:

<https://eprints.whiterose.ac.uk/193708/>

Version: Accepted Version

Proceedings Paper:

Zhang, J., Liu, W. orcid.org/0000-0003-2968-2888, Tennant, A. et al. (3 more authors) (2022) Performance evaluation of spatial scattering modulation in the indoor environment. In: 2022 International Symposium on Wireless Communication Systems (ISWCS). Proceedings of 2022 International Symposium on Wireless Communication Systems (ISWCS), 19-22 Oct 2022, Hangzhou, China. Institute of Electrical and Electronics Engineers (IEEE) . ISBN 9781665455459

<https://doi.org/10.1109/iswcs56560.2022.9940429>

© 2022 The Authors. This accepted manuscript version is available under a Creative Commons Attribution CC BY licence. (<http://creativecommons.org/licenses/by/4.0>)

Reuse

This article is distributed under the terms of the Creative Commons Attribution (CC BY) licence. This licence allows you to distribute, remix, tweak, and build upon the work, even commercially, as long as you credit the authors for the original work. More information and the full terms of the licence here:

<https://creativecommons.org/licenses/>

Takedown

If you consider content in White Rose Research Online to be in breach of UK law, please notify us by emailing eprints@whiterose.ac.uk including the URL of the record and the reason for the withdrawal request.



eprints@whiterose.ac.uk
<https://eprints.whiterose.ac.uk/>

Performance Evaluation of Spatial Scattering Modulation in the Indoor Environment

Jiliang Zhang^{1,2}, Wei Liu², Alan Tennant², Weijie Qi¹, Jiming Chen¹, and Jie Zhang^{1,2}

1. Department of R&D, Ranplan Wireless Network Design Ltd., Cambridge, UK.

2. Department of Electronic and Electrical Engineering, The University of Sheffield, Sheffield, UK.

Abstract—In this paper, a state-of-the-art massive MIMO modulation system, spatial scattering modulation (SSM), is evaluated considering practical indoor wireless environments for the first time. Firstly, the SSM system is reviewed, which works under the narrowband sparse physical channel model and exploits beamspace domain resources to enhance spectral efficiency via analog beamforming. Secondly, to generate parameters for the narrowband sparse physical channel model in a specific indoor environment, channel prediction is performed based on the intelligent ray launching algorithm (IRLA), which has been verified via practical measurements. Therein, building structures and large objects in the indoor environment are modelled. Thirdly, an approach is proposed for characterizing ergodic average bit error probability (ABEP) to evaluate the SSM system in the indoor environment. Finally, numerical experiments are carried out, which show that channel models widely adopted in existing literature for evaluations of the SSM system are oversimplified.

Index Terms—Spatial scattering modulation, massive MIMO, analog beamforming, intelligent ray launching algorithm, indoor radio wave propagation, bit error probability.

I. INTRODUCTION

Massive multiple-input-multiple-output (MIMO) technologies have been widely employed in wireless communication systems [1]. As a strong candidate for B5G modulation systems with massive MIMO antenna arrays at both the transmitter and the receiver, spatial scattering modulation (SSM) has been proposed and widely investigated to minimize power consumption as it requires only one radio frequency (RF)-chain at the transmitter [2]–[8]. In the SSM system, the information bits are separated into two streams. One is modulated via selecting the direction of multipath (MP) components to efficiently exploit the beamspace domain resource via analog beamforming. The other is carried by transmitted amplitude and phase modulation (APM) symbols.

Without considering practical wireless radio propagation environments, proof-of-principle evaluation for the SSM system has been studied based on narrowband sparse physical channel models. In most existing works, channel gains of MP components are assumed to be independent and identically distributed (i.i.d.) complex Gaussian variables [2]–[8]. However,

the distribution of channel gains for different MP components could neither be i.i.d. nor Gaussian in a practical scenario. Therefore, there is a need to evaluate and compare SSM systems before deployment in a more practical environment.

To this end, environmental factors should be taken into account carefully in the performance analysis for the SSM system. Especially, evaluation of SSM systems in an indoor environment is crucial as most wireless traffics take place indoors [11]–[13]. In the indoor environment, building structures have strong interaction with propagating radio waves [14], [15], and therefore affect the performance of indoor SSM significantly.

Either practical measurement or deterministic channel modelling can be employed in the evaluation of wireless systems considering the specific indoor environment. Practical measurement can provide a deterministic answer to the practical performance of modulation systems, such as in the case of spatial modulation systems [17]–[23]. However, a clear challenge in practical measurement is its extremely high cost and complexity. As an alternative, the deterministic channel model is a powerful tool to evaluate the performance of SSM systems [24]. Realized by PC-based computing, deterministic channel models facilitate performance evaluation traversing the whole environment and thus provide a more comprehensive understanding of the performance of SSM systems. Currently, to our best knowledge, the systematic deterministic channel model-based evaluation of indoor SSM systems has not been reported in the literature yet.

In this work, we fill this gap by focusing on the evaluation of the SSM system in indoor environments based on the indoor intelligent ray launching algorithm (IRLA) [24], which achieves a good tradeoff between computational burden and channel prediction accuracy. As the effectiveness of IRLA has been verified via practical measurements [25], [26], with the capability of traversing the whole environment, IRLA can provide an alternative to practical measurements in a specific indoor environment. The contribution of this paper is summarized as follows.

- IRLA-based channel prediction is carried out for the considered indoor environment. Channel parameters for 952 massive MIMO links are generated to facilitate comprehensive SSM evaluation.
- An approach is proposed for characterizing ergodic ABEP via traversing the whole considered environment.

This research was a part of KTP project - “Massive MIMO Beamforming for 5G”, which is funded by UKRI through Innovate UK.

For the purpose of open access, the authors have applied a Creative Commons Attribution (CC BY) license to any Author Accepted Manuscript version arising.

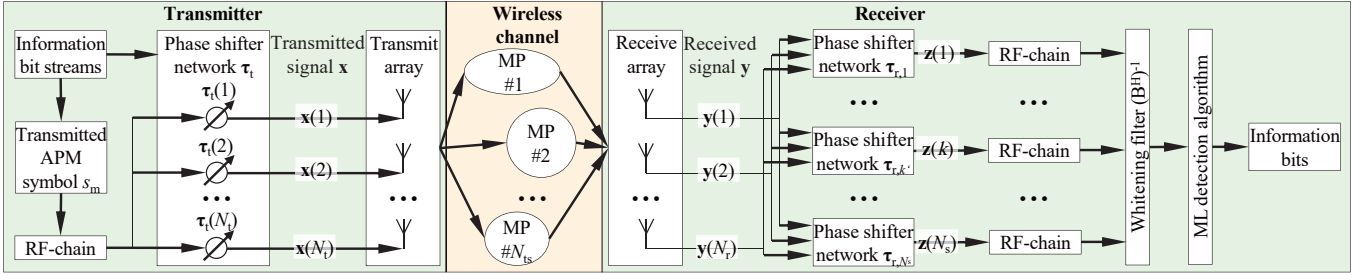


Fig. 1. The system model of SSM.

TABLE I
NOTATIONS

Notations	Definitions
N_t	Number of antenna elements in the transmit antenna array
N_r	Number of antenna elements in the receive antenna array
n_t	Indices of transmit antenna elements
n_r	Indices of receive antenna elements
\mathbf{H}	The MIMO channel matrix
N_{ts}	Total number of multipath components
n_s	The n_s -th scattering path
$\tilde{\mathbf{H}}_{n_s}$	Channel matrix of the n_s -th MP component
$\tilde{\mathbf{H}}$	Effective channel matrix
β	The channel gain of multipath components
θ_t	The AoD of multipath components
θ_r	The AoA of multipath components
\mathbf{x}	The vector of transmitted signal
\mathbf{a}_t	Array vectors at the transmitter
\mathbf{a}_r	Array vectors at the receiver
$\boldsymbol{\tau}_t$	Beam-steering vector at the transmitter
$\boldsymbol{\tau}_r$	Beam-steering vector at the receiver
N_s	Total number of the candidate multipath components
M	Modulation order of the transmitted symbol
s_m	The m -th point in the signal constellation
k	The selected multipath components at the transmitter
$(\cdot)^H$	Complex conjugate transpose operator
N_l	The number of total measured links in IRLA
n_l	Indices of measured links in IRLA
$\text{chol}(\cdot)$	Cholesky factorization of a matrix
$\text{Tr}(\cdot)$	Trace of a matrix
$E[\cdot]$	Expectation operator
$Q(\cdot)$	The Q -function

- Numerical experiments are performed to validate our approach by comparing it with existing SSM evaluations. It shows that existing channel models are oversimplified in evaluating the SSM system. The performance of the SSM system is also investigated with various parameters such as modulation orders, number of antennas, number of candidate MP components, etc.

The remaining part is structured as follows. The system model of SSM is described in Section II. Channel prediction in a typical indoor environment is presented in Section III. The evaluation approach for the SSM system is introduced in Section IV. Numerical results are provided in Section V and conclusions are drawn in Section VI. Notations of this paper are summarized in TABLE I.

II. SYSTEM MODEL

A. Channel model

Before introducing the system model shown in Fig. 1 [3], we elaborate on channel models adopted in this paper. Assume that both the transmitter (Tx) and the receiver (Rx) are equipped with uniform linear antenna arrays (ULAs) and all elements in the Tx and Rx arrays are omnidirectional and vertically polarized for simplicity. The Tx array and the Rx array have N_t and N_r elements, respectively. Thus, the transmission from the Tx array to the Rx array can be expressed as

$$\mathbf{y} = \sqrt{\frac{\rho}{N_t}} \mathbf{H} \mathbf{x} + \mathbf{n}_a, \quad (1)$$

where ρ is the SNR at the receiver, \mathbf{H} is the channel matrix with a dimension of $N_r \times N_t$, \mathbf{x} is the $N_t \times 1$ transmitted signal vector, \mathbf{y} is the $N_r \times 1$ received signal vector, and $\mathbf{n}_a \sim \mathcal{CN}(\mathbf{0}, \mathbf{I})$ is the $N_r \times 1$ noise vector. \mathbf{H} is normalized to $E[\text{Tr}(\mathbf{H}^H \mathbf{H})] = N_t N_r$.

The narrowband sparse physical channel is adopted in this paper [3]. A link-level indoor channel is composed by N_{ts} MP components with different channel gains, angles of departure (AoDs), and angles of arrival (AoAs). The channel matrix is given by [28]

$$\mathbf{H} = \sum_{n_s=1}^{N_{ts}} \beta(n_s) \tilde{\mathbf{H}}_{n_s}, \quad (2)$$

where β is the descendingly sorted channel gain vector with a dimension of $N_{ts} \times 1$. Its n_s -th element, denoted by $\beta(n_s)$, is the channel gain from the Tx array to the Rx array via the n_s -th MP component. $\tilde{\mathbf{H}}_{n_s}$ is the normalized channel matrix from the Tx array to the Rx array via the n_s -th MP component.

$$\tilde{\mathbf{H}}_{n_s} = \mathbf{a}_{t n_s}^H \mathbf{a}_{r n_s}. \quad (3)$$

$\mathbf{a}_{t n_s}$ and $\mathbf{a}_{r n_s}$ are Tx and Rx array steering vectors [3], respectively. The n_t -th element of $\mathbf{a}_{t n_s}$ and the n_r -th element of $\mathbf{a}_{r n_s}$ are, respectively, computed by

$$\mathbf{a}_{t, n_s}(n_t) = e^{j \frac{2\pi}{\lambda} (n_t - 1) d_t \cos \theta_t(n_s)} \quad (4)$$

and

$$\mathbf{a}_{r, n_s}(n_r) = e^{j \frac{2\pi}{\lambda} (n_r - 1) d_r \cos \theta_r(n_s)}, \quad (5)$$

where λ denotes the wavelength of the radio wave. $\boldsymbol{\theta}_t$ is the AoD vector with a dimension of $N_{ts} \times 1$. Its n_s -th element, denoted by $\theta_t(n_s)$, is the AoD of the n_s -th MP component. Similarly, $\boldsymbol{\theta}_r$ is the AoA vector. d_t and d_r denote adjacent spacing of Tx and Rx antenna elements, respectively.

B. Transmitter

The transmitter employs only one RF chain to reduce energy consumption, following the idea of spatial modulation [29]. In an SSM transmission link, the transmitter divides a bit block into streams and transmits them simultaneously. The first stream is conveyed by the selection of MP components via analog beamforming, while the second stream by the selection of transmitted amplitude-and-phase-modulated (APM) symbol.

To transmit the first stream, Tx generates a pencil beam steering to a selected MP component. In this process, channel state information (CSI) is assumed to be known at the transmitter following the setup of typical SSM systems [3]–[6], [8]. If R_{mp} bits are transmitted in this stream, the Tx array select one MP component out of $N_s = 2^{R_{mp}}$ candidate MP components with $N_s \leq N_{ts}$. When more MP components are available, i.e., $N_s < N_{ts}$, we choose MP components with N_s greatest channel gain to maximize the received power.

To generate the pencil beam to the k -th MP component, a transmit phase shifter network is applied, where each phase shifter is connected to one Tx antenna element. The response of the phase shifter network is denoted by

$$\boldsymbol{\tau}_{t,k} = \mathbf{a}_{t,k}^H. \quad (6)$$

The transmit phase shifter network is fed by an APM signal s_m , which is amplified by the single RF-chain. Therefore, the transmitted symbol \mathbf{x} in (1) can be represented as

$$\mathbf{x} = \boldsymbol{\tau}_{t,k} s_m. \quad (7)$$

To transmit the second stream, s_m is selected from an APM constellation with M candidate symbols, such as M -phase shift keying and quadrature amplitude modulation M -QAM. As such, the data rate of the second stream is $R_{sy} = \log_2 M$.

The total data rate for an SSM transmission is then $R = R_{mp} + R_{sy} = \log_2(MN_s)$.

C. Receiver

At the Rx, the received signal is computed by substituting (7) into (1)–(3).

$$\begin{aligned} \mathbf{y} &= \sqrt{\frac{\rho}{N_t}} \mathbf{H} \boldsymbol{\tau}_{t,k} s_m + \mathbf{n}_a \\ &= \sqrt{\frac{\rho}{N_t}} \sum_{n_s=1}^{N_{ts}} \beta(n_s) \tilde{\mathbf{H}}_{n_s} \boldsymbol{\tau}_{t,k} s_m + \mathbf{n}_a \\ &= \sqrt{\frac{\rho}{N_t}} \sum_{n_s=1}^{N_{ts}} \beta(n_s) \mathbf{a}_{tn_s}^H \mathbf{a}_{rn_s} \boldsymbol{\tau}_{t,k} s_m + \mathbf{n}_a. \end{aligned} \quad (8)$$

The received signal \mathbf{y} is filtered by N_s Rx phase shifter networks, and fed into N_s Rx RF-chain with low noise

amplifiers (LNAs). By assuming that Rx knows perfect CSI via channel estimation, each pair of Rx phase shifter network and Rx RF-chain is associated with one candidate MP component.

To maximize the SNR at the RF chain, each Rx phase shifter network steers a pencil beam to its associated candidate MP component. That is, for the k' -th candidate MP component, the Rx phase shifter network is set as

$$\boldsymbol{\tau}_{r,k'} = \mathbf{a}_{r,k'}. \quad (9)$$

Denote the output signal of RF chains as \mathbf{z} . Then, the output signal of the k' -th RF chain, $\mathbf{z}(k')$, is computed by combining (9) and (8).

$$\begin{aligned} \mathbf{z}(k') &= \boldsymbol{\tau}_{r,k'} \mathbf{y} \\ &= \sqrt{\frac{\rho}{N_t}} \sum_{n_s=1}^{N_{ts}} \beta(n_s) \boldsymbol{\tau}_{r,k'} \mathbf{a}_{tn_s}^H \mathbf{a}_{rn_s} \boldsymbol{\tau}_{t,k} s_m + \boldsymbol{\tau}_{r,k'} \mathbf{n}_a. \end{aligned} \quad (10)$$

To simplify the derivation of the optimal detection algorithm, an $N_s \times N_s$ effective channel matrix $\bar{\mathbf{H}}$ is defined [10]. The element at the k -th row and k' -th column of $\bar{\mathbf{H}}$, denoted by $\bar{\mathbf{H}}(k', k)$, is given by

$$\bar{\mathbf{H}}(k', k) = \sqrt{\frac{1}{N_t}} \sum_{n_s=1}^{N_{ts}} \beta(n_s) \boldsymbol{\tau}_{r,k'} \mathbf{a}_{tn_s}^H \mathbf{a}_{rn_s} \boldsymbol{\tau}_{t,k}. \quad (11)$$

By combining (10) and (11), we have

$$\mathbf{z} = \sqrt{\rho} \bar{\mathbf{H}}(:, k) s_m + \bar{\mathbf{n}}, \quad (12)$$

where $\bar{\mathbf{H}}(:, k)$ is the k -th row of $\bar{\mathbf{H}}$. $\bar{\mathbf{n}} = \boldsymbol{\tau}_{r,k'} \mathbf{n}_a$ is an additive colored Gaussian noise with a covariance matrix $\mathbf{C}_{\text{noise}}$, whose element $\mathbf{C}_{\text{noise}}(k'_1, k'_2) = \boldsymbol{\tau}_{r,k'_1} \boldsymbol{\tau}_{r,k'_2}^H$. A simplified expression was given in [10, Lemma 1].

Equation (12) is the same as the system model of conventional spatial modulation with additive colored Gaussian noise [22, Eq. (1)]. Then, applying a whitening filter and with the maximal likelihood (ML) detection, the optimal SSM detector is given by

$$[\hat{k}, \hat{m}] = \arg \min_{k, m} \left\| (\mathbf{B}^H)^{-1} (\mathbf{z} - \sqrt{\rho} \bar{\mathbf{H}}(:, k) s_m) \right\| \quad (13)$$

where matrix \mathbf{B} is obtained by Cholesky factorization of $\mathbf{C}_{\text{noise}}$, i.e.,

$$\mathbf{B} = \text{chol}(\mathbf{C}_{\text{noise}}). \quad (14)$$

D. Summary of assumptions

We summarize the following main assumptions applied in this paper.

- The narrowband sparse physical channel is adopted [3].
- Both Tx and Rx arrays are assumed to be ULAs.
- All elements in the Tx and Rx arrays are assumed to be omnidirectional and vertically polarized.
- CSI is assumed to be known at the transmitter as in typical SSM systems [3]–[8].

It is worth noting that breaking each of the above assumptions deserves a comprehensive study. Without dragging the readers out of the scope of this paper, we apply the above assumptions throughout this paper.

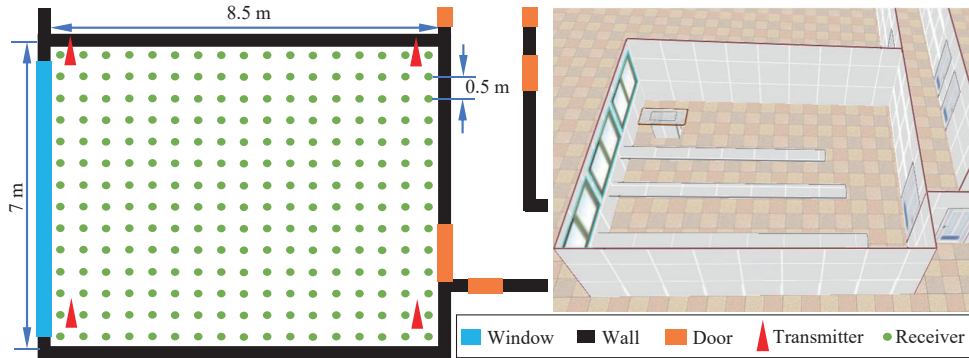


Fig. 2. A typical indoor environment for SSM performance evaluation.

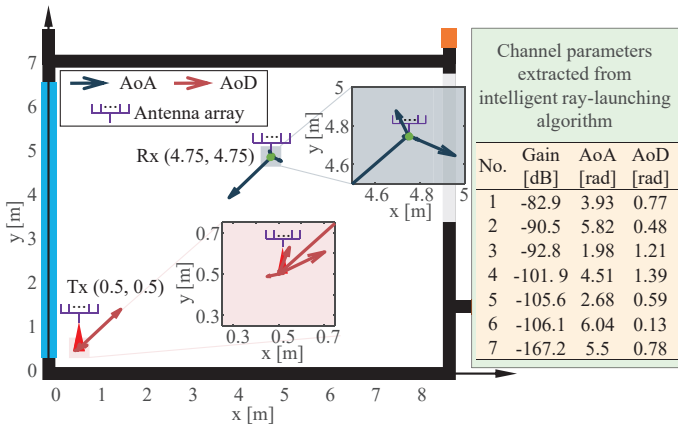


Fig. 3. An example of the IRLA-based channel prediction, where Tx and Rx locate at (0.5, 0.5) and (4.75, 4.75), respectively.

III. THE INDOOR ENVIRONMENT AND CHANNEL PREDICTION

The indoor environment under consideration is illustrated in Fig. 2. For the sake of simplicity, we only consider building structures and large objects, such as walls, windows, floors, ceilings, doors, and desks, and ignore small ones, such as chairs and screens. As mentioned earlier, the IRLA is applied to predict indoor propagation channels, and the resolution is set as 0.5 m to achieve a good tradeoff between computational complexity and prediction accuracy.

There are four Tx antenna arrays, located at four corners of the room, respectively. The IRLA slices the propagation environment into small cube units with a dimension of 0.5 m \times 0.5 m \times 0.5 m, and predicts channels between the Tx and centers of all cubes. The height of both Tx and Rx is set as 1 m above the floor. The Rx array visits all cube centers with a height of 1 m and computes the ergodic performance of SSM accordingly.

With 4 Tx positions and 238 Rx positions, there are $N_l = 952$ links in total. The index of a link is denoted by $n_l \in \{1, 2, \dots, 952\}$. In the n_l -th channel prediction, we obtain channel parameters including 1) the number of MP components N_{ts,n_l} , 2) the path loss of each MP component

TABLE II
PARAMETERS IN NUMERICAL RESULTS

Parameter	Description	Value
N_r	Number of Rx antennas	16
N_t	Number of Tx antennas	32
d_t	Spacing of Tx antenna elements	0.5λ
d_r	Spacing of Rx antenna elements	0.5λ
N_s	Number of candidate MP components	2
M	Modulation order	4

β_{n_l} with a length of N_{ts,n_l} , 3) AoD of each MP component θ_{t,n_l} at the Tx with a length of N_{ts,n_l} , and 4) AoA of each MP component θ_{r,n_l} at the Rx with a length of N_{ts,n_l} .

In the example shown in Fig. 3, Tx and Rx are located at (0.5,0.5) and (4.75,4.75), respectively. Seven MP components are present in this link. For all the other links, the IRLA is applied to extract channel parameters with the same data format.

IV. BIT ERROR PERFORMANCE EVALUATION

In this section, we elaborate on how to evaluate the ergodic bit error performance of the SSM system with IRLA-based channel predictions.

First, we explain the evaluation approach for an SSM transmission under the n_l -th channel prediction with N_{ts,n_l} , β_{n_l} , θ_{t,n_l} and θ_{r,n_l} .

It is well known that analytical derivation of the exact average bit error probability (ABEP) with fading channels for complex modulation systems is challenging. Therefore, the approximate union upper bound on the ABEP is derived as (15) at the bottom of the next page [27], where $N(k, m, \hat{k}, \hat{m})$ denotes the number of bits in error when k and m are transmitted at Tx but \hat{k} and \hat{m} are detected at Rx. $P_{n_l}(k, m, \hat{k}, \hat{m})$ is the pairwise error probability, which is defined as the probability that, when k and m are transmitted but \hat{k} and \hat{m} are detected assuming only candidates (k, m) and (\hat{k}, \hat{m}) can be selected at Tx.

A closed-form expression of $P(k, m, \hat{k}, \hat{m})$ can be computed as (16) at the bottom of the next page, where \mathbf{B}_{n_l} and \mathbf{H}_{n_l} are obtained by replacing $(N_{ts}, \beta, \theta_t, \theta_r)$ by $(N_{ts,n_l}, \beta_{n_l}, \theta_{t,n_l}, \theta_{r,n_l})$ in (11) and (14), respectively. As the derivation of

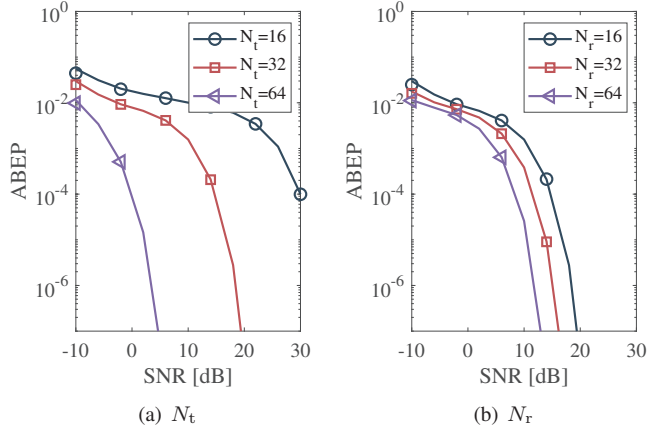


Fig. 4. Ergodic ABEP with different scales of antenna array.

(16) is straightforward following most references in this paper, the proof is omitted here to save space.

Then, the closed-form upper bound on the $ABEP_{n_1}$ for the n_1 -th measurement link is obtained by substituting (16) into (15).

The ergodic ABEP, that characterizes the ABEP performance under this specific indoor scenario is computed by

$$ABEP = \frac{1}{N_1} \sum_{n_1=1}^{N_1} ABEP_{n_1}. \quad (17)$$

By traversing the entire environment, (17) can be used as the performance indicator of the SSM system in the considered indoor environment.

V. NUMERICAL RESULTS

In this section, performance of the SSM system is studied based on the ABEP upper bound. The simulation parameters are given in Table II unless otherwise specified. In all figures in this section, the solid lines are closed-form ABEP upper bounds computed by (17), and markers are simulation results. We will see that the analytical results and the simulation results match each other well.

The impact of antenna array size on the ergodic ABEP is shown in Fig. 4. It can be seen that the ergodic ABEP can be effectively reduced by increasing the size of the antenna array at either Tx or Rx. Nevertheless, the ABEP can be reduced more effectively by increasing the number of Tx antennas. An intuitive explanation is that if the Tx antenna array is insufficiently large, the energy of the radio wave will spread in

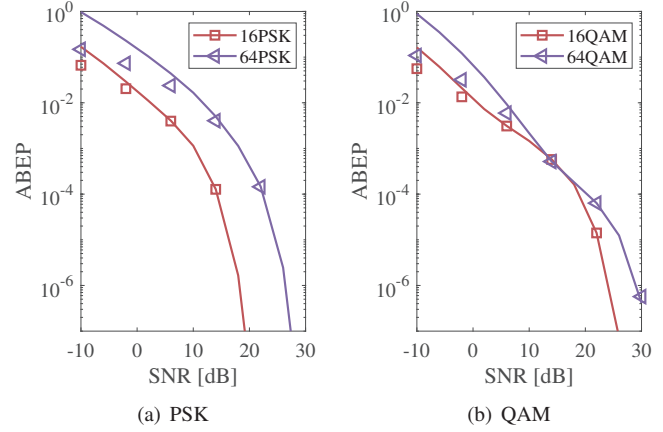


Fig. 5. Ergodic ABEP with different modulation orders.

space without focusing on any MP component, which reduces the effective signal energy to the receiver. In this condition, even with a large Rx antenna array, the receiver SNR is still low. In contrast, if the Tx antenna array is large, the majority of the energy of the transmitted signal can reach the Rx via an MP component. As a result, even with a small antenna array, Rx is still able to demodulate the signal effectively.

In Fig. 5, we illustrate the impact of modulation order on the ergodic ABEP. An interesting observation is that with the SSM system with PSK constellation can outperform that with QAM constellation, similar to the case of an SM system [30]. This is due to the interaction of signal constellation and MP component selection, and the ABEP of SSM depends on the Euclidean distance with joint detection errors of \hat{m} and \hat{k} . As PSK is a constant-modulus modulation that facilitates simpler modulation and demodulation than QAM, we recommend employing the PSK constellation in the SSM system.

In Fig. 6, the impact of the number of candidate MP components, N_s , on the ergodic ABEP is presented. It can be seen that the ABEP performance of SSM is very sensitive to N_s . This is because the MP component with low channel gain is more likely to be selected to transmit signals with a larger N_s . If the beam is steered to an MP component with a very weak channel gain, demodulation of the APM symbols could suffer from very low receive power and the overall ergodic ABEP will be significantly increased.

In Fig. 7, the ergodic ABEP obtained from both IRLA channel prediction and i.i.d complex Gaussian channel models

$$ABEP_{n_1} \leq \sum_{k=1}^{N_s} \sum_{\hat{k}=1}^{N_s} \sum_{m_1=1}^M \sum_{\hat{m}_1=1}^M \frac{N(k, m, \hat{k}, \hat{m}) P_{n_1}(k, m, \hat{k}, \hat{m})}{N_s M \log_2(N_s M)}, \quad (15)$$

$$P_{n_1}(k, m, \hat{k}, \hat{m}) = Q \left(\sqrt{\frac{\rho}{2}} \left\| \left(\mathbf{B}_{n_1}^H \right)^{-1} \left(\bar{\mathbf{H}}_{n_1}(:, k) s_m - \bar{\mathbf{H}}_{n_1}(:, \hat{k}) s_{\hat{m}} \right) \right\| \right). \quad (16)$$

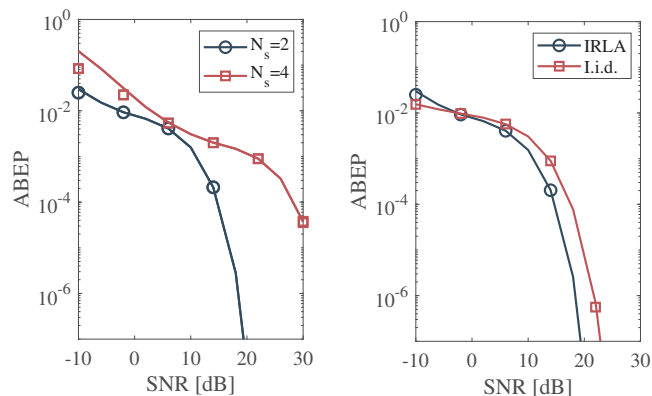


Fig. 6. Ergodic ABEP with different number of candidate MP components. Fig. 7. Ergodic ABEP under different channel models.

is provided. In the i.i.d. simulation, we apply the same AoA and AoD as in IRLA, and randomly generate channel gain β_0 as i.i.d complex Gaussian variables. As shown, the i.i.d. complex Gaussian channel model systematically underestimates the performance of SSM systems due to different distribution of channel gains.

VI. CONCLUSIONS

Considering practical indoor environments, the emerging SSM system is evaluated in terms of ergodic ABEP based on channel predictions using IRLA. Numerical results show that channel models employed for SSM systems in current literature systematically underestimate the performance of SSM systems. If the SSM systems are deployed under the guidance of these ideal channel models, the resultant cost and energy consumption due to deploying more than enough wireless devices would be unnecessarily high. Therefore, a more systematic evaluation based on deterministic channel models is essential before deploying SSM systems in an indoor environment in the future.

REFERENCES

- [1] E. G. Larsson et al., "Massive MIMO for next generation wireless systems," *IEEE Commun. Mag.*, vol. 52, no. 2, pp. 186-195, Feb. 2014.
- [2] J. Zhang et al., "Generalized polarization-space modulation," *IEEE Trans. Commun.*, vol. 68, no. 1, pp. 258-273, Jan. 2020.
- [3] Y. Ding et al., "Spatial scattering modulation for uplink millimeter-wave system," *IEEE Commun. Lett.*, vol. 21, no. 10, pp. 2178-2181, Jul. 2017.
- [4] Y. Ding et al., "Millimeter wave adaptive transmission using spatial scattering modulation," *IEEE Int. Conf. Commun.*, pp. 1-6, May 2017.
- [5] Y. Tu et al., "Generalized spatial scattering modulation for uplink millimeter wave MIMO system," *IEEE/CIC Int. Conf. Commun. in China*, pp. 22-27, Aug. 2018.
- [6] S. Ruan et al., "Diversity analysis for spatial scattering modulation in millimeter wave MIMO system," *IEEE Int. Conf. Wireless Commun. Signal. Process.*, pp. 1-5, Sep. 2019.
- [7] J. Zhang "Adaptive spatial scattering modulation," *IEEE Trans. Wireless. Commun.*, vol. 20, no. 10, pp. 6680-6690, Oct. 2021
- [8] Q. Li et al., "Polarized spatial scattering modulation," *IEEE Commun. Lett.*, vol. 23, no. 12, pp. 2252-2256, Dec. 2019.
- [9] O. Ayach et al., "Spatially sparse precoding in millimeter wave MIMO systems," *IEEE Trans. Wireless. Commun.*, vol. 13, no. 3, pp. 1499-1513, Mar. 2014.
- [10] Y. Jiang et al., "Generalized 3-D spatial scattering modulation," *IEEE Trans. Wireless. Commun.*, vol. 21, no. 3, pp. 1570-1585, March 2022.

- [11] J. Zhang et al., "Fundamental wireless performance of a building," *IEEE Wireless Commun.*, vol. 29, no. 1, pp. 186-193, Feb. 2022.
- [12] J. Zhang et al., "Wireless performance evaluation of building layouts: Closed-form computation of figures of merit," *IEEE Trans. Commun.*, vol. 69, no. 7, pp. 4890-4906, July 2021.
- [13] J. Zhang et al., "Wireless energy efficiency evaluation for buildings under design based on analysis of interference gain," *IEEE Trans. Veh. Technol.*, vol. 69, no. 6, pp. 6310-24, June 2020.
- [14] Y. Zhang et al., "How friendly are building materials as reflectors to indoor LOS MIMO communications?" *IEEE Internet Things J.*, vol. 7, no. 9, pp. 9116-9127, Sep. 2020.
- [15] Y. Zhang et al., "Lower-bound capacity-based wireless friendliness evaluation for walls as reflectors," *IEEE Trans. Broadcast.*, vol. 67, no. 4, pp. 917-924, Dec. 2021.
- [16] Y. Zhang et al., "Effects of wall reflection on the per-antenna power distribution of ZF-precoded ULA for indoor mmWave MU-MIMO transmissions," *IEEE Commun. Lett.*, vol. 25, no. 1, pp. 13-17, Jan. 2021.
- [17] N. Serafimovski et al., "Practical implementation of spatial modulation," *IEEE Trans. Veh. Technol.*, vol. 62, no. 9, pp. 4511-4523, Nov. 2013.
- [18] X. Zhu et al., "On the performance of 3-D spatial modulation over measured indoor channels," *IEEE Trans. Veh. Technol.*, vol. 71, no. 2, pp. 2110-2115, Feb. 2022.
- [19] A. Younis et al., "Performance of spatial modulation using measured real-world channels," *IEEE 78th Veh. Technol. Conf.*, Sep. 2013, pp. 1-5.
- [20] O. Hiari et al., "First hardware implementation of an SSK MIMO system with no RF-Chain at the transmitter," *IEEE Trans. Ind. Electron.*, vol. 68, no. 5, pp. 4477-4484, May 2021.
- [21] P. Liu et al., "Performance of generalized spatial modulation MIMO over measured 60 GHz indoor channels," *IEEE Trans. Commun.*, vol. 66, no. 1, pp. 133-148, Jan. 2018.
- [22] J. Zhang et al., "Bit error probability of spatial modulation over measured indoor channels," *IEEE Trans. Wireless. Commun.*, vol. 13, no. 3, pp. 1380-1387, March 2014.
- [23] J. Zhang et al., "Performance of spatial modulation with constant transmitted power under LOS and NLOS scenarios," *IEEE International Conference on Communications (ICC)*, 2015, pp. 2750-2755.
- [24] Z. Lai et al., "Intelligent ray launching algorithm for indoor scenarios," *Radioengineering*, vol. 20, no. 2, pp. 398-408, June 2011.
- [25] W. Yang et al., "Verification of an intelligent ray launching algorithm in indoor environments in the Ka-band," *Radio Science*, vol. 56, no. 9, pp. 1-11, Sept. 2021.
- [26] W. Yang et al., "Indoor measurement based verification of ray launching algorithm at the Ka-band," *XXXIIIrd General Assembly and Scientific Symposium of the International Union of Radio Science*, 2020, pp. 1-4.
- [27] M. K. Simon and M. Alouini, *Digital communication over fading channels*, Hoboken, NJ, USA: Wiley, 2005.
- [28] A. Goldsmith, *Wireless communications*, Cambridge, UK: Cambridge University Press, 2005.
- [29] R. Y. Mesleh et al., "Spatial modulation," *IEEE Trans. Veh. Technol.*, vol. 57, no. 4, pp. 2228-2241, July 2008.
- [30] M. Di Renzo and H. Haas, "Bit error probability of SM-MIMO over generalized fading channels," *IEEE Trans. Veh. Technol.*, vol. 61, no. 3, pp. 1124-1144, March 2012.